An iterative dual energy CT reconstruction method for a K-edge contrast material

M. Depypere[1], J. Nuyts[2], N. van Gastel[3], G. Carmeliet[3], F. Maes[1] and P. Suetens[1]

[1]Medical Image Computing (ESAT/PSI), [2]Department of Nuclear Medicine,
[3]Department for Experimental Medicine and Endocrinology,
K.U.Leuven, Leuven, Belgium

ABSTRACT

We present and evaluate an iterative dual energy CT reconstruction algorithm for a K-edge contrast material in microCT imaging. This allows improved discrimination of contrast enhanced structures such as vasculature from surrounding bony structures. The energy dependence of the attenuation is modeled by decomposing the linear attenuation coefficient into three basis functions. Any material without a K-edge in the imaging energy range can be modeled by two basis functions describing the Compton scatter and the photoelectric effect respectively. A K-edge material is described by using its mass attenuation coefficient as third basis function. During reconstruction the basis function coefficients are determined for each voxel of the image by maximizing the likelihood of the data. The relative weights of the Compton and photoelectric components are constrained to those of expected materials to reduce the number of unknowns to two per voxel. The proposed method is validated on simulated and real microCT projections. The presented method was found to perform better than a typical post-reconstruction approach with respect to beam-hardening and noise at the expense of increased computation time.

1. INTRODUCTION

Dual energy CT enables discrimination of materials with similar linear attenuation coefficients. It has been widely used to distinguish bone from vascular contrast agents that contain elements with a K-edge in the imaging energy range, such as iodine, barium or lead. Post-reconstruction decomposition techniques first reconstruct the different sets of projection data and then extract the material fractions by decomposing the attenuation into material components.[1,2] In pre-reconstruction methods the measured line integrals are converted to basis function integrals, and these are reconstructed into basis function coefficients.[3,4] Such methods are computationally simple, but are sensitive to noise[5,6] and beam hardening.[7]

Both noise and beam hardening can be problematic when using a micro-computed tomography (microCT) system to image vasculature around bony tissue in small animals. Limiting radiation dose to prevent radiation effects is essential for in vivo experiments and negatively influences the noise. For ex vivo measurements, obtaining images with high signal-to-noise ratio can require cumbersome long scan durations, and heat dissipation issues. In addition, blood vessels filled with highly dense contrast agent or the presence of metal implants can cause significant beam hardening artifacts. This application would benefit from a dual energy algorithm that is robust to noise and beam hardening.

Iterative dual energy methods allow modeling the noise and the energy dependence of the attenuation coefficient, and can therefore be expected to yield better signal-to-noise ratios and to cope better with dense materials than post-reconstruction approaches. Existing iterative dual energy techniques are either unable to deal with K-edge elements[8] or require a third measurement[9] or the use of photon-counting detectors,[10] that are not yet widely available. We propose an iterative dual energy reconstruction algorithm that allows a K-edge element to be present in the object and that requires only two spectral measurements.

2. METHOD

Polychromatic attenuation model Beam hardening artifacts are caused by the faulty assumption that the X-ray beam in microCT systems is monochromatic, while dual energy applications attempt to exploit the dependency of the linear attenuation coefficient on the photon energy. Reducing beam hardening and differentiating materials with similar attenuation coefficients both benefit from using a polychromatic model to account for the

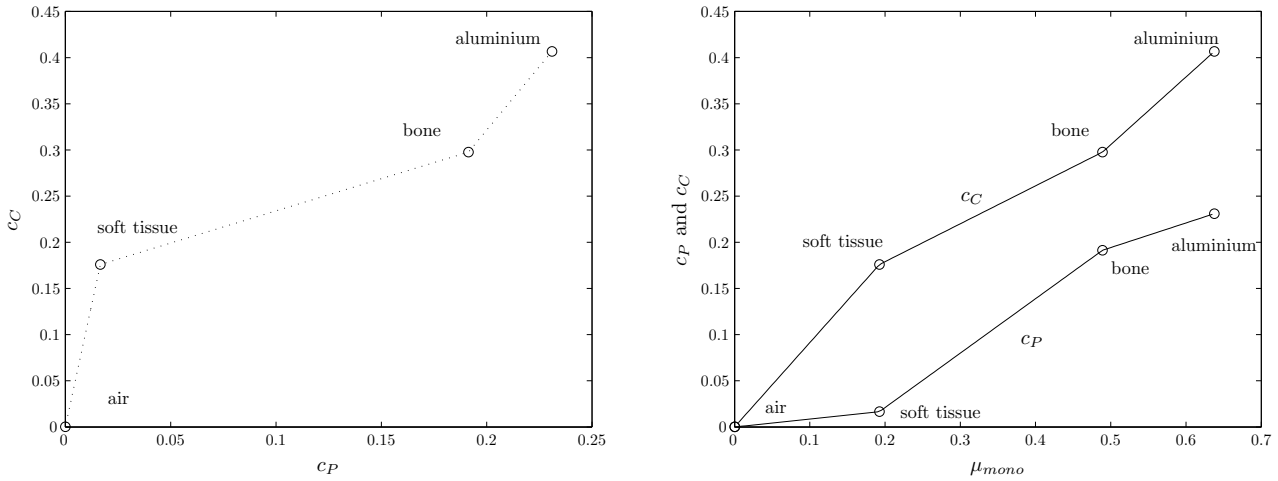

(a) (b)

Figure 1: Illustration of the material assumptions for the set of base substances [air, soft tissue, bone, aluminium]. (a) Photoelectric coefficient versus Compton scatter coefficient. (b) Monochromatic linear attenuation coefficient at 70 keV versus Photoelectric coefficient and Compton scatter.

energy spectrum of the X-ray beam and of the material attenuation. The dependence of the linear attenuation coefficient μ on the photon energy E can be described by a linear combination of basis functions $\alpha(E)$

$$\mu(E) = \sum_b c_b \alpha_b(E) \tag{1}$$

It has been shown that 2 basis functions are enough to approximate all materials without a K-edge in the imaging energy range. A well-known set of basis functions are the photoelectric interactions α_P and Compton scattering α_C.[3] To describe the attenuation of a voxel containing a single element with a K-edge in the imaging energy range, a third basis function modeling the mass attenuation coefficient of the K-edge material α_K has to be added.

$$\mu(E) \approx c_P \alpha_P(E) + c_C \alpha_C(E) + c_K \alpha_K(E) \tag{2}$$

Solving Equation 2 for the fractions c_P, c_C and c_K requires three measurements at different energies. These measurements can be obtained by taking a third CT scan,[9] or in a single scan by using multi-bin photon counting detectors.[10] We adopt the approach of De Man et al. and restrict the relative weights of the photoelectric and compton components based on material assumptions.[11]

The coefficients c_P and c_C of basis functions α_P and α_C are plotted in Figure 1a (circles) for some materials without K-edge we can expect in a biomedical microCT scan. The coefficients are computed by applying a least squares fit of Equation 2 to the known energy dependent attenuation coefficient (data from the National Institute of Standards and Technology) of these materials. Voxels containing a single material without K-edge should be assigned a pair of coefficients (c_P, c_C) equal to the corresponding combination for this material. At tissue borders, partial volume voxels can be expected to contain multiple materials. We assume that all voxels in the image contain, in addition to a possible K-edge material, a combination of not more than 2 adjacent base materials (air, soft tissue), (soft tissue, bone), (bone, aluminium), such that only combinations of c_P and c_C that lie on the dotted line in Figure 1a are allowed. Under this assumption, the relationship between c_P and c_C can be approximated by a piecewise-linear curve defined by a set of base materials. For more details about this model, we refer to De Man et al.[11]

In addition, for our choice of base materials, both c_P and c_C are monotonic functions of the monochromatic attenuation at a reference energy μ_{mono} (Figure 1b). As a result, μ_{mono} defines both c_P and c_C via a set of base

materials, for example [air, soft tissue, bone, aluminium].

$$\mu(E) \approx c_P(\mu_{mono})\alpha_P(E) + c_C(\mu_{mono})\alpha_C(E) + c_K\alpha_K(E) \tag{3}$$

As these are only two sets of unknowns (μ_{mono}, c_K) in each voxel, the solution can be found with just two measurements at different energies.

Iterative reconstruction method The goal of the reconstruction is to determine the values of μ_{mono} and c_K in every voxel that maximize the log-likelihood of the projection data. The loglikelihood L of a Poisson noise model is given by

$$L = \sum_i y_i \ln(\bar{y}_i) - \bar{y}_i \tag{4}$$

with y_i the acquired noisy sinogram ray i, and $\bar{y}_i$ the expected sinogram ray i.

The expected sinogram is computed with the polychromatic model presented by De Man et al.[11]

$$\bar{y}_i = \sum_k b_{ik} e^{-\sum_j l_{ij}\mu_{jk}} \tag{5}$$

with k the energy index and b_{ik} the total energy detected by detector i in absence of an object for photons with energy k. b_{ik} models the source spectrum and the detector sensitivity and is considered known as it can be computed from the scanner characteristics. l_{ij} is the intersection length of sinogram ray i with voxel j, and μ_{jk} is the discretized $\mu(E)$ in voxel j at energy index k:

$$\mu_{jk} = c_P(\mu_{mono,j})\alpha_{P,k} + c_C(\mu_{mono,j})\alpha_{C,k} + c_{K,j}\alpha_{K,k} \tag{6}$$

The likelihood is iteratively maximized by updating μ_{mono} and c_K in voxel j with the update steps presented by Nuyts et al:[12]

$$\Delta\mu_{mono,j} = -\frac{\frac{\partial L}{\partial \mu_{mono,j}}}{\sum_h \frac{\partial^2 L}{\partial \mu_{mono,j}\partial \mu_{mono,h}} + \sum_h \frac{\partial^2 L}{\partial \mu_{mono,j}\partial c_{K,h}}} \tag{7}$$

$$\Delta c_{K,j} = -\frac{\frac{\partial L}{\partial c_{K,j}}}{\sum_h \frac{\partial^2 L}{\partial c_{K,j}\partial c_{K,h}} + \sum_h \frac{\partial^2 L}{\partial c_{K,j}\partial \mu_{mono,h}}} \tag{8}$$

In all experiments, the reconstruction is initialized with a uniform image, performs 50 iterations and is sped up with ordered subsets.[13]

Post-reconstruction method For comparison with the proposed iterative reconstruction method, we have implemented the dual energy post-reconstruction method of Granton et al.[14] The two projection data sets acquired at energy E_i are reconstructed separately by filtered backprojection (FBP). For every voxel that consists of three additive base materials, the following set of equations is valid

$$\mu(E_1) = f_1\mu_1(E_1) + f_2\mu_2(E_1) + f_3\mu_3(E_1) \tag{9}$$

$$\mu(E_2) = f_1\mu_1(E_2) + f_2\mu_2(E_2) + f_3\mu_3(E_2) \tag{10}$$

$$1 = f_1 + f_2 + f_3 \tag{11}$$

with f_m the tissue fractions and $\mu_m(E_i)$ the attenuation of base material m. The set of equations is solved for f_m for every image voxel using non-negative least squares,[14] as tissue fractions cannot be negative. The attenuation of the different substances at each energy $\mu_m(E_i)$ is computed from a manually delineated, representative region in the appropriate reconstruction.

3. RESULTS

Three experiments are conducted on different simulated and real data sets comparing our iterative approach and the post-reconstruction approach. The simulations were performed with the same settings as used for the real scans. The low energy scan used settings 50kV tube voltage and 0.5mm aluminium filtration, while the high energy scan put the tube voltage at 100kV and used a filter of 0.5mm aluminium and 0.038mm copper. These filters were used because they are installed by default on our SkyScan 1172 microCT system (SkyScan, Kontich, Belgium).

Simulation The first experiment validates the theoretical framework by reconstructing simulated, noiseless projections of a virtual phantom. The simulation modeled the spectrum, material attenuation and detector, while ignoring noise or scatter. The phantom consists of a circular 'water' region, with two circular 'bone' regions, and two smaller circular 'contrast agent' regions. The contrast agent is a mixture of water and barium sulfate with 0.15 and 0.2 gram barium sulfate per ml mixture in the two regions respectively, but could be based on any other K-edge material such as lead or iodine. The results are shown in Figure 2. Beam hardening in the FBP reconstruction of the 50kV scan induces streak artifacts (Figure 2a). These artifacts influence the material fraction decomposition and some water voxels are falsely attributed a barium sulfate component(Figure 2b). The iterative method suffers less from beam hardening due to its spectral model (Figure 2c), and decomposes the mass volume fractions of the barium sulfate components (Figure 2d) as 0.1455g/ml $\pm$ 0.0021 and 0.1957g/ml $\pm$ 0.0024 (mean $\pm$ standard deviation in region of interest) where we expect 0.15 and 0.20g/ml respectively.

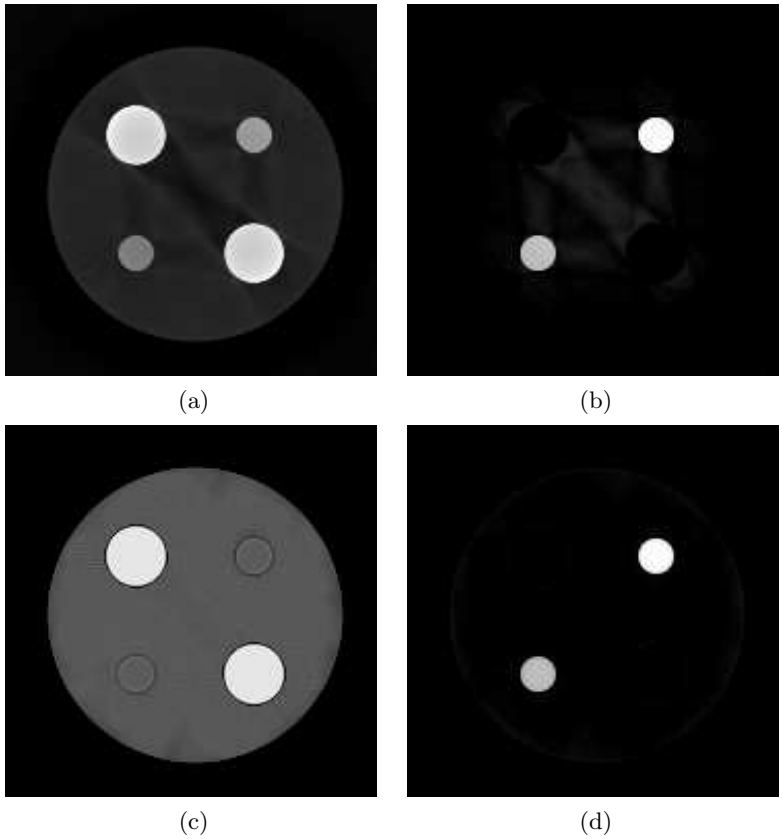

(a) (b) (c) (d)

Figure 2: Results of the simulation containing water, bone and barium sulfate. (a) FBP reconstruction of the 50kV image. (b) Barium sulfate tissue fractions as estimated by the post-reconstruction approach. (c) Monochromatic reconstruction μ_{mono} of the iterative method at 70kV, without the barium sulfate component. (d) The barium sulfate component c_K as computed by the iterative method.

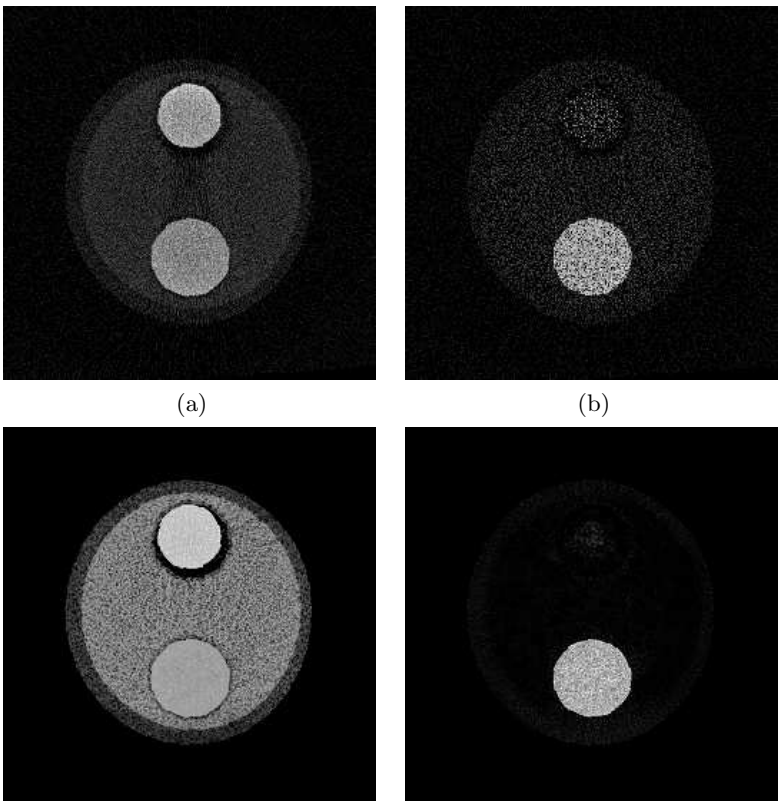

Figure 3: Results of the phantom. (a) FBP reconstruction of the 50kV image. (b) Barium sulfate tissue fractions as estimated by the post-reconstruction approach. (c) Monochromatic reconstruction μ_{mono} of the iterative method at 70kV, without the barium sulfate component. (d) The barium sulfate component c_K as computed by the iterative method.

Phantom The second experiment investigates the influence of realistic noise conditions by acquiring microCT projections of a phantom. A polypropylene tube filled with water contains a mix of barium sulfate, water and gelatine to prevent sedimentation, and a cylinder of bone equivalent material, calcium hydroxyapatite (CaHA). The FBP reconstruction is noisy (Figure 3a), and the tissue decomposition results in a coefficient of variation of 0.36 in the barium sulfate region (Figure 3b). The iterative approach is more robust to noise in these conditions with a coefficient of variation of 0.15 in the same region (Figure 3c and d). Due to the inhomogeneity of the CaHA, some particles exhibit K-edge behaviour and are detected as such by both methods.

Mouse tibia Finally the method is tested on an ex vivo mouse tibia perfused with barium sulfate. In the FBP reconstruction of Figure 4a, the two large grey structures represent bone, while the white dots are cross sections of blood vessels perfused with barium sulfate. Due to noise, the post-reconstruction decomposition considers several bone voxels as contrast agent (Figure 4b), while the iterative approach does not suffer from this issue (Figure 4c). The vasculature can be interpreted more easily when viewed as a red overlay on the FBP reconstruction (Figure 4d).

4. CONCLUSION

We have presented an iterative dual energy maximum likelihood reconstruction algorithm, that is able to deal with one K-edge material. Hence, our method provides the ability to discriminate contrast enhanced structures such as vasculature from surrounding bony structures. The algorithm is based on a relationship between two

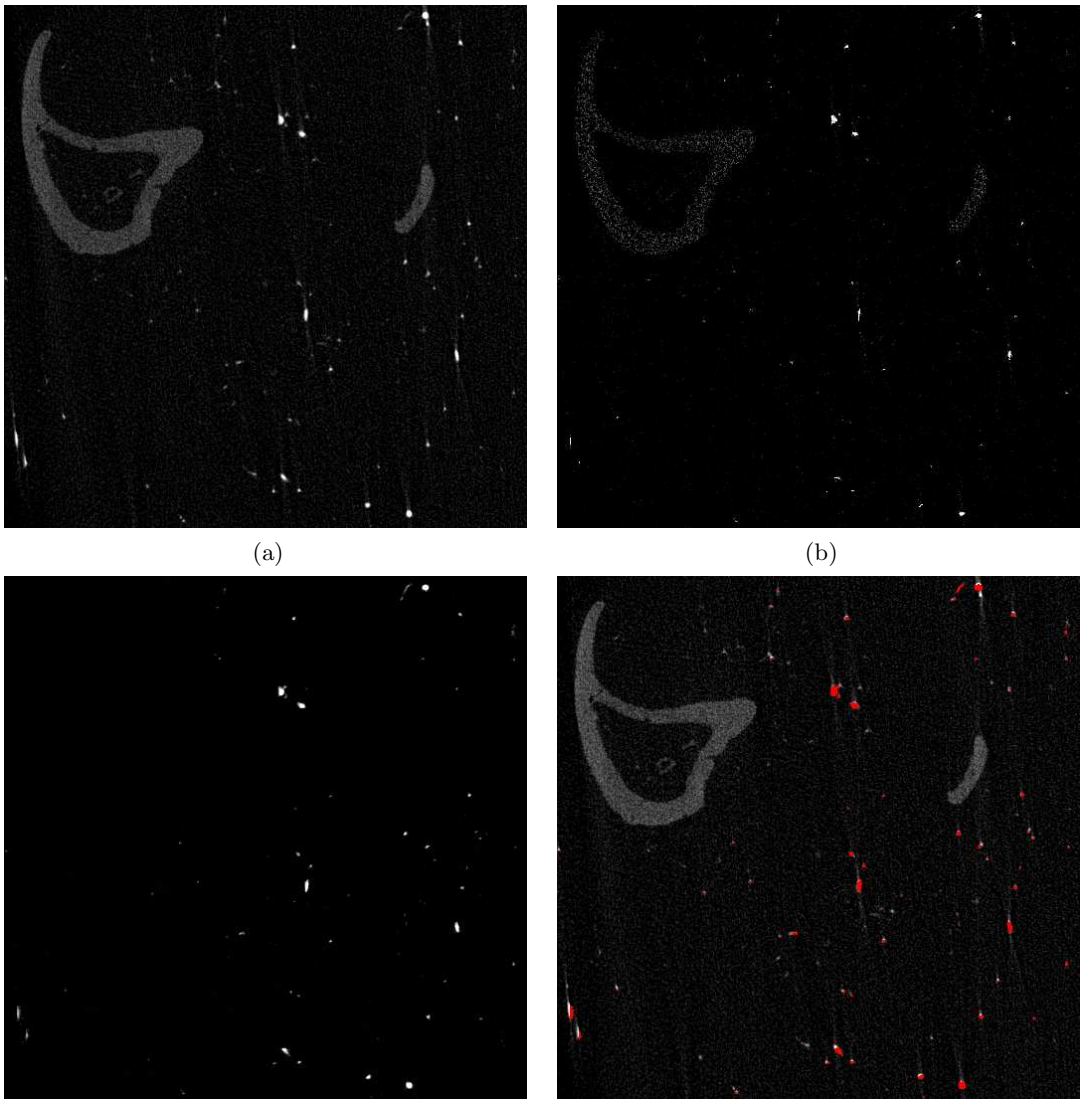

(a) (b)

(c) (d)

Figure 4: Results of the mouse tibia. (a) FBP reconstruction of the 50kV image. (b) Barium sulfate tissue fractions as estimated by the post-reconstruction approach. (c) The barium sulfate component c_K as computed by the iterative method. (d) Overlay of the contrast c_K in red on (a).

of the three basis functions describing the energy dependence of the linear attenuation coefficient. We adopt the relationship between Compton and photoelectric coefficients of common substances presented by De Man et al.[11] This relationship is then applied to parametrize the Compton and photoelectric basis functions with a single value per voxel. By reducing the number of unknowns to two per reconstruction voxel, this approach does not require a third scan or a photon counting detector and can therefore be applied to any kind of CT scanner. The algorithm is validated on simulated and real microCT images of bone and barium sulfate contrast agent. The method performs better than a typical post-reconstruction approach with respect to beam-hardening and noise at the expense of increased computation time.

REFERENCES

1. Kelcz, F., Joseph, P. M., and Hilal, S. K., "Noise considerations in dual energy ct scanning," *Medical Physics* **6**(5), 418–425 (1979).
2. Vinegar, H. J. and Wellington, S. L., "Tomographic imaging of three-phase flow experiments," *Review of Scientific Instruments* **58**(1), 96–107 (1987).
3. Alvarez, R. E. and Macovski, A., "Energy-selective reconstructions in X-ray Computerised Tomography," *Physics in Medicine & Biology* **21**(5), 733–744 (1976).
4. Riederer, S. J. and Mistretta, C. A., "Selective iodine imaging using k-edge energies in computerized x-ray tomography," *Medical Physics* **4**(6), 474–481 (1977).
5. Kalender, W., Klotz, E., and Kostaridou, L., "An algorithm for noise suppression in dual energy ct material density images," *IEEE Transactions on Medical Imaging* **7**, 218–224 (Sep 1988).
6. Heismann, B. J. and Balda, M., "Noise transfer analysis of base material decomposition methods," *Medical Imaging 2007: Physics of Medical Imaging* **6510**(1), 651011, SPIE (2007).
7. Walter, D. J., Tkaczyk, E. J., and Wu, X., "Accuracy and precision of dual energy ct imaging for the quantification of tissue fat content," *Medical Imaging 2006: Physics of Medical Imaging* **6142**(1), 61421G, SPIE (2006).
8. Sukovic, P. and Clinthorne, N., "Penalized weighted least-squares image reconstruction for dual energy X-ray transmission tomography," *IEEE Transactions on Medical Imaging* **19**(11), 1075–1081 (2000).
9. Sukovic, P. and Clinthorne, N., "Basis material decomposition using triple-energy x-ray computed tomography," in [*Instrumentation and Measurement Technology Conference*], **3**, 1615–1618 vol.3 (1999).
10. Roessl, E. and Proksa, R., "K-edge imaging in X-ray computed tomography using multi-bin photon counting detectors," *Physics in Medicine and Biology* **52**(15), 4679–4696 (2007).
11. De Man, B., Nuyts, J., Dupont, P., G., M., and Suetens, P., "An iterative maximum-likelihood polychromatic algorithm for CT," *IEEE Transactions on Medical Imaging* **20**(10), 999–1008 (2001).
12. Nuyts, J., De Man, B., Dupont, P., Defrise, M., Suetens, P., and Mortelmans, L., "Iterative reconstruction for helical CT: a simulation study," *Physics in Medicine & Biology* **43**(4), 729–737 (1998).
13. Hudson, H. M. and Larkin, R. S., "Accelerated image reconstruction using ordered subsets of projection data," *IEEE Transactions on Medical Imaging* **13**(4), 601–609 (1994).
14. Granton, P. V., Pollmann, S. I., Ford, N. L., Drangova, M., and Holdsworth, D. W., "Implementation of dual- and triple-energy cone-beam micro-ct for postreconstruction material decomposition," *Medical Physics* **35**(11), 5030–5042 (2008).